Japanese Journal of Applied Physics **54**, 08KA07 (2015) **REGULAR PAPER**
http://dx.doi.org/10.7567/JJAP.54.08KA07

Molecular beam epitaxial growth of intermediate-band materials based on GaAs:N δ-doped superlattices

Tomoya Suzuki[1]*, Kazuki Osada[1], Shuhei Yagi[1]*, Shunya Naitoh[2], Yasushi Shoji[2], Yasuto Hijikata[1], Yoshitaka Okada[2], and Hiroyuki Yaguchi[1]

[1]*Graduate School of Science and Engineering, Saitama University, Saitama 338-8570, Japan*
[2]*Research Center for Advanced Science and Technology (RCAST), The University of Tokyo, Meguro, Tokyo 153-8904, Japan*
E-mail: tsuzuki@opt.ees.saitama-u.ac.jp; yagi@opt.ees.saitama-u.ac.jp

Received December 19, 2014; revised March 19, 2015; accepted March 23, 2015; published online July 10, 2015

We fabricated GaAs:N δ-doped superlattices (SLs) by molecular beam epitaxy and investigated their potential as an intermediate-band photoabsorber in high-efficiency solar cells. The N area concentration in a N δ-doped layer was well controlled by adjusting the fabrication conditions, and the SLs with the average N composition of up to 1.5% were obtained. The SL minibands related to the N-induced E_+ and E_- conduction subbands were formed with well-separated bottom energies of up to 0.4 eV, indicating the suitability of this material system for use in intermediate-band solar cells. A two-step photoabsorption process in a solar cell with the SL absorber was successfully demonstrated through external quantum efficiency measurements under additional infrared illumination at room temperature.

1. Introduction

In recent years, many researchers have attempted to improve the efficiency of solar cells above the Shockley–Queisser limit,[1)] and the intermediate-band solar cell (IBSC) is one such attempt.[2–18)] Intermediate-band (IB) energy structures can be realized by introducing an allowed state in the forbidden band of a host semiconductor, which enables below-bandgap photon absorption by a two-step electron transition from the valence band (VB) to the conduction band (CB) via the IB states. The output voltage of an IBSC is limited by the quasi-Fermi level split between the CB and the VB if proper electrical separation of the IB states in the absorber from the contact layers is achieved. The maximum efficiency of the IBSC is theoretically estimated to reach 63% under optimum bandgap configurations.[2)]

A key issue in the development of IBSCs is how to fabricate an ideal IB material. A small amount of nitrogen (N) incorporation into GaAs leads to CB splitting into two subbands, E_+ and E_-.[19–24)] Since these E_+ and E_- bands and the VB are expected to constitute a multiband structure, the application of GaAsN to IBSCs has been studied.[14–17)] Recently, we proposed GaAs:N δ-doped superlattices (SLs), in which N δ-doped layers are periodically inserted into GaAs with a period of several nm, as alternative materials of uniformly N-doped GaAsN alloys for use in IBSCs.[25,26)] In the SL structures, the N-induced conduction subbands are formed in the vicinity of the N δ-doped layers. Each of the E_+ and E_- bands composes a periodic potential with the CB of spacer GaAs, resulting in the formation of multiple minibands above and below the GaAs CB edge, respectively. We found that optical transitions originating from the SL minibands related to the E_+ band are strongly enhanced compared with those from the E_+ band in uniformly N-incorporated GaAsN alloys.[25–27)] This suggests that the SL structures are more promising candidates for the absorber of IBSCs.

In previous work, we fabricated GaAs:N δ-doped SLs by metalorganic vapor phase epitaxy (MOVPE). In MOVPE growth, the growth temperature is required to be kept above the thermal decomposition temperature of source gases. This limits the maximum N composition of the SL to be ~0.2% on average and the energy separation between the bottoms of the E_+- and E_--related minibands to be below ~0.2 eV. In terms of energy band configuration as an IB absorber, the energy separation corresponds to the CB–IB gap and should be larger (e.g., the optimum CB–IB gaps are 0.5 and 0.7 eV for the IBSCs with the CB–VB gaps of 1.48 and 1.93 eV, respectively).[2)] Our estimation of the conversion efficiency of IBSCs with the SL absorber using the Krönig–Penney model and the detailed-balance model indicated that the optimum value of the average N composition in the SL is within the range of 3 to 4%,[26)] and thus the present value needs to be much higher. In this study, we have fabricated GaAs:N δ-doped SLs having higher N composition of up to 1.5% by molecular beam epitaxy (MBE). Their potential as an IB absorber will be discussed referring to the results of the structural and optical characterizations. In the final part of the paper, we will show the photovoltaic characterization of an IBSC using a GaAs:N δ-doped SL, including a demonstration of a two-step photoabsorption process under multiple-wavelength illumination.

2. Experimental procedure

The samples were grown on GaAs(001) substrates by solid-source MBE. Metal Ga and As were used as the Ga and As sources, respectively. An active nitrogen source was supplied through an RF N_2-plasma cell. A N δ-doped layer was formed in such a way that the growing surface was exposed to active nitrogen while temporarily stopping GaAs growth, followed by GaAs cap growth. By repeating the alternate formation of a N δ-doped layer and a GaAs spacer layer, 20-period SL structures were fabricated. In addition, a solar cell containing a 20-period SL inserted in the i-region of a p–i–n structure was fabricated to evaluate the photovoltaic properties. A reference cell in which i-GaAs is grown instead of the SL was also prepared for comparison.

X-ray diffraction (XRD) and secondary ion mass spectroscopy (SIMS) were used for structural evaluation. Photoreflectance (PR) measurements were carried out to investigate the energy structures. In the PR measurements, a diode-pumped solid-state (DPSS) laser at 532 nm was used as modulation light. The probe light was illuminated onto the surface of the samples from a halogen lamp through a

monochromator. PR signals were detected by a Si photodiode using a phase-sensitive lock-in amplification system. For the solar cell structures, current–voltage (J–V) measurements under 1-sun light illumination (AM1.5, 100 mW/cm^2) and external quantum efficiency (EQE) measurements were carried out at room temperature (RT). As a demonstration of the two-step photoabsorption process through the electron transition from the VB to E_+ miniband via the E_- miniband (corresponding to the IB), EQE under additional infrared (IR) (>1.4 μm) illumination generated from a 1-sun light source through an IR pass filter was measured. To evaluate quantitatively the contribution of the two-step photoabsorption process to photocurrent generation, the spectral dependence of ΔEQE, which is defined as the difference in EQE measured with and without additional IR illumination,[10,11] was discussed.

3. Results and discussion

3.1 Effects of fabrication conditions on N incorporation into δ-doped layers

First, the effects of the substrate temperature and N exposure time during the formation of a N δ-doped layer on the incorporated N concentration were investigated. A number of N δ-doped layers formed under various conditions were inserted into a GaAs layer. The N exposure time and substrate temperature during the δ-doped layer formation were changed in the ranges of 15 to 180 s and 420 to 580 °C, respectively. The substrate temperature was controlled to a target value before starting the N exposure and was held through the following GaAs cap growth. Figure 1(a) shows a schematic illustration of the sample structure and the N concentration profile measured by SIMS. Sharp N concentration peaks were confirmed at the positions of the N δ-doped layers. The N area concentration in each δ-doped layer was estimated by integrating each concentration peak along the depth direction. The N area concentration in a δ-doped layer increased monotonically and approached a saturation value with increasing N exposure time at a constant substrate temperature, as shown in Fig. 1(b). Figure 1(c) indicates the dependence of the N area concentration on the substrate temperature for the δ-doped layers formed with the N exposure time of 60 s. The N area concentration was of the order of 10^{14} cm^{-2} at substrate temperatures from 460 to 540 °C, whereas the value was 1 order of magnitude smaller for a higher substrate temperature. The N adsorption rate on the growing surface is determined by the balance between the supplied N flux and the desorption rate of the N adsorbed on the surface. Therefore, the abrupt reduction of the N content at the higher temperature suggests that the N desorption from the surface becomes dominant at that temperature range. On the basis of these results, we fabricated SL structures at a constant substrate temperature of 500 °C, and the N area concentration was controlled by changing the N exposure time.

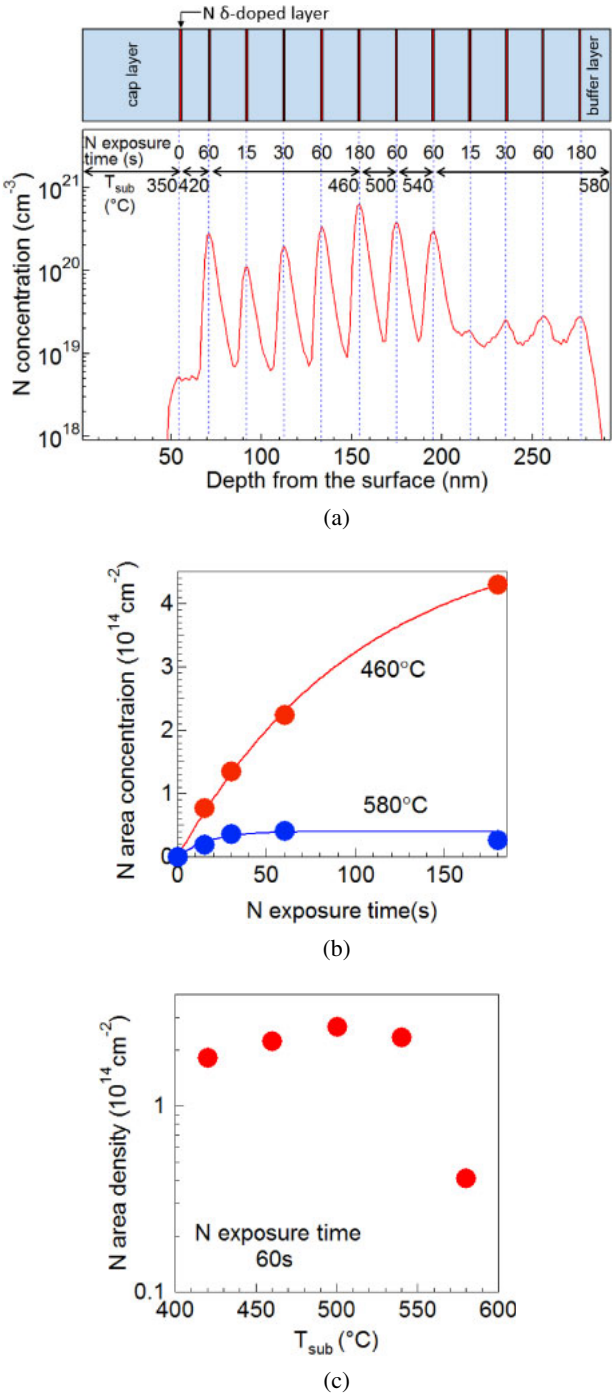

Fig. 1. (Color online) (a) SIMS profile of N in GaAs containing a number of N δ-doped layers formed under various conditions. The N exposure time and substrate temperature during δ-doped layer formation were changed in the ranges of 15 to 180 s and 420 to 580 °C, respectively. (b) Dependence of the N area concentration in a δ-doped layer on the N exposure time at substrate temperatures of 460 and 580 °C. The lines are guides for the eye. (c) Substrate temperature dependence of the N area concentration in N δ-doped layers.

3.2 Structural and optical characterizations of GaAs:N δ-doped SLs

Figure 2 shows XRD patterns of the fabricated SLs with a nominal period of 6 nm. The N exposure time during the formation of the δ-doped layer for the SLs was changed from 10 to 120 s. It is confirmed that clear SL satellite peaks appear in the patterns. The SL periods estimated from the 1st-order satellite peak angles indicated that the deviation from the nominal value was within 0.1 nm for these samples. A longer N exposure time leads to a higher 0th-order satellite peak angle, i.e., a higher N concentration. X-ray reciprocal space mapping around the asymmetric (224) reflection was also measured and the results revealed that these SLs were fully

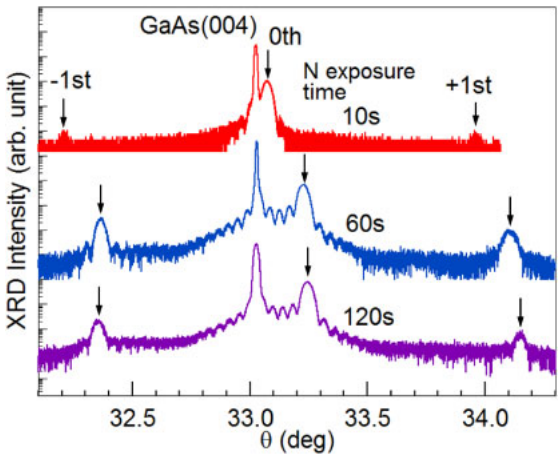

Fig. 2. (Color online) θ–2θ XRD patterns of GaAs:N δ-doped SLs around GaAs(004) reflection. The N exposure times during δ-doped layer formation for these SLs were 10, 60, and 120 s.

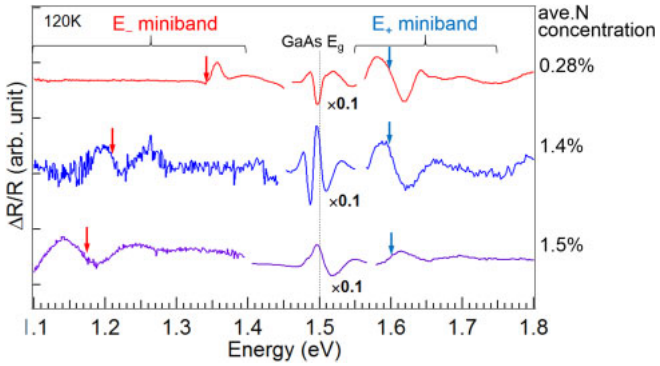

Fig. 3. (Color online) PR spectra of GaAs:N δ-doped SLs with average N compositions of 0.28, 1.4, and 1.5%. The arrows indicate the bottom energies of the SL minibands estimated from the spectra.

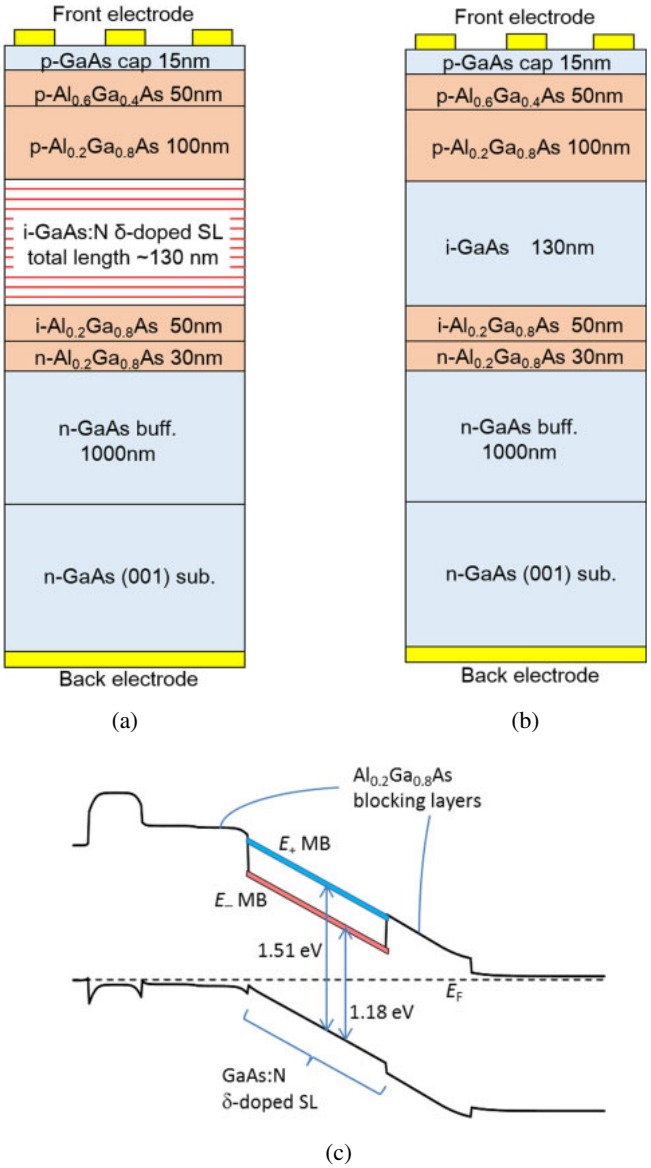

Fig. 4. (Color online) Schematic illustrations of (a) the solar cell with a GaAs:N δ-doped SL and (b) the reference cell. The SL period and the average N composition of the SL are 6.1 nm and 1.1%, respectively. (c) A calculated energy band diagram of the SL cell. In the calculation, the SL layer was treated as a GaAsN layer with the same E$_-$ energy level as that at E$_-$ miniband (MB) bottom of the SL.

strained on GaAs. The lattice constants of the fully relaxed SLs were estimated from the 0th satellite peak angles in the XRD patterns using the elastic constants of GaAs. The average N composition in each SL was calculated from them by assuming Vegard's law between GaAs and cubic GaN, and was 0.28, 1.4, and 1.5% for the SLs with the N exposure times of 10, 60, and 120 s, respectively. Therefore, we have succeeded in increasing nitrogen uptake to about 1 order of magnitude larger than that of SLs fabricated by MOVPE in our previous works.

Furthermore, we observed the formation of an IB structure in these SLs by PR spectroscopy at 120 K. Figure 3 shows the PR spectra. The PR signals at around 1.50 eV are due to the GaAs bandgap transition in the cap, buffer layers, or substrates. The PR spectra clearly represented the optical transitions originating from E$_+$- and E$_-$-related SL minibands observed at 1.55–1.75 and 1.1–1.4 eV, respectively. The arrows in the figure indicate the bottom energies of each miniband estimated by fitting with the Aspnes third-derivative functional form.[28] The E$_+$ and E$_-$ minibands showed a blueshift and a redshift with increasing N concentration, respectively. In terms of IB energy structure, the E$_+$ and E$_-$ minibands correspond to the CB and the IB, respectively, and their bottoms are energetically well separated (>0.25–0.4 eV) from each other, indicating the suitability of this material system for use in IBSCs. Detailed discussions of the structural dependence of the energy configuration in the SLs are given in our other publications.[29,30]

3.3 IBSC characterization

Photovoltaic characterization of the solar cell containing a GaAs:N δ-doped SL was carried out. Figures 4(a) and 4(b) show schematic illustrations of the solar cell with a GaAs:N δ-doped SL and the reference cell with the same structure as the SL cell except for not containing N-doped layers, respectively. The SL cell has 20 periods of N δ-doped layers separated by 6.1-nm-thick GaAs spacers in the i-region. The N area concentration in a δ-doped layer and the average N concentration in the SL were 1.4×10^{14} cm^{-2} and 1.1%, respectively. 50-nm-thick $Al_{0.6}Ga_{0.4}As$ was inserted in the p-region as a window layer. In addition, $Al_{0.2}Ga_{0.8}As$ layers were grown on both sides of the SL as carrier blocking layers

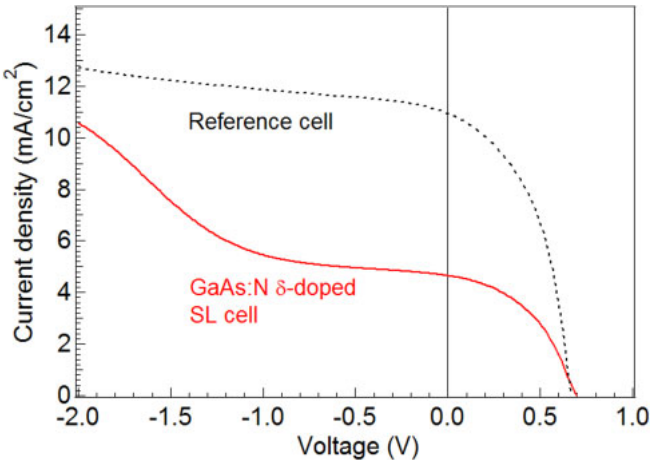

Fig. 5. (Color online) *J*–*V* curves of the SL cell and the reference cell.

Table I. Photovoltaic parameters of the fabricated solar cells.

	Short-circuit current density (mA/cm^2)	Open-circuit voltage (V)	Fill factor	Conversion efficiency (%)
SL cell	4.65	0.70	0.44	1.43
Reference cell	10.9	0.67	0.47	3.44

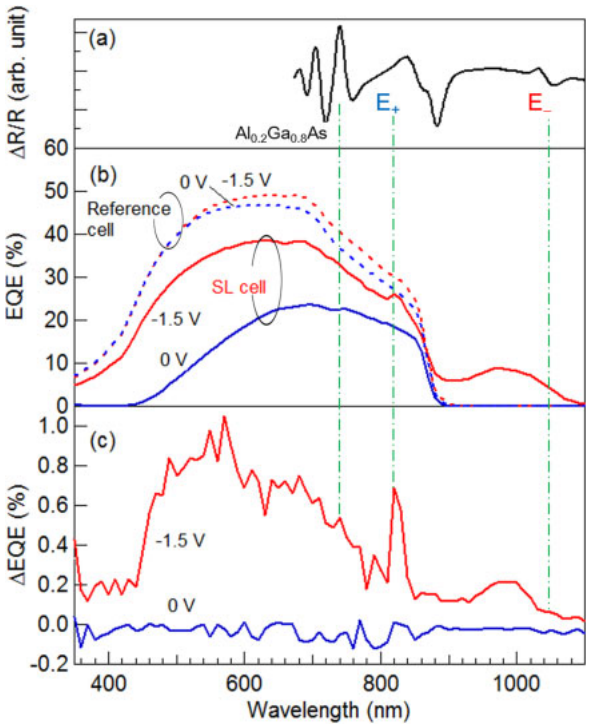

Fig. 6. (Color online) (a) PR, (b) EQE, and (c) ΔEQE spectra of the SL cell. The EQE and the ΔEQE spectra were taken at a reverse bias of 1.5 V as well as under the short-circuit condition. The EQE spectra of the reference cell are also shown in (b).

to suppress direct electron transport between the E_- miniband (IB) and the contact layers. The electrical separation of the IB from the contact layers is a key factor in the ideal IBSC operation, as mentioned in Sect. 1. Antireflection coating was not applied to the cells. A band diagram of the SL cell calculated using a one-dimensional (1D) Poisson solver[31] is illustrated in Fig. 4(c). In the calculation, the SL layer was treated as a GaAsN layer with the same E_- energy level as the E_- miniband bottom of the SL. The energy positions of the minibands in the SL were determined by the spectral properties of the SL, which will be indicated later.

Figure 5 shows the *J*–*V* curves of the SL cell and the reference cell under 1-sun illumination. Table I summarizes the parameters of these solar cells determined from the *J*–*V* curves. The short-circuit current density (J_{sc}) and open-circuit voltage (V_{oc}) of the SL cell were 4.65 mA/cm^2 and 0.70 V, respectively. Although the J_{sc} of the SL cell was about half that of the reference cell, the V_{oc} of the SL cell was slightly higher than that of the reference cell. The output current of the SL cell increased with increasing reverse bias voltage, particularly for reverse bias over 1 V.

Figures 6(a), 6(b), and 6(c) show PR, EQE, and ΔEQE spectra of the SL cell measured at RT, respectively. The PR spectrum of the SL cell represented the transition signals related to the GaAs (~880 nm) and AlGaAs (<750 nm) layers. In addition, transitions originating from E_+ and E_- minibands in the SL were observed at about 820 and 1050 nm, respectively. The EQE and ΔEQE spectra were taken at a reverse bias of 1.5 V as well as under the short-circuit condition. The EQE spectra of the reference cell are also shown in Fig. 6(b). Under the short-circuit condition, the SL cell presented almost no photoresponse in the wavelength ranges shorter than 400 nm and longer than 900 nm in the EQE spectrum. The absence of the photoresponse above 900 nm and a slight increase in the V_{oc} of the SL cell may indicate that efficient electronic separation of the E_- miniband (IB) from the contact layers and selective carrier collection from the E_+ miniband (CB) are achieved. However, the lower EQE in the whole wavelength range compared with that of the reference cell, which is consistent with the smaller J_{sc} of the SL cell, suggests a shorter diffusion length and a dominant recombination loss of photoelectrons in the N-containing layer. By the application of reverse bias, the EQE of the SL cell was drastically increased to the level comparable to that of the reference cell. The absorption edge was extended to ~1100 nm owing to the E_- miniband (IB) absorption and the following carrier extraction with the assistance of the electric field. In addition, a small EQE peak appeared at about 820 nm, which corresponds to the E_+ miniband (CB) transition energy. Therefore, it is confirmed that photoabsorption and carrier generation related to both E_+ and E_- minibands occurred in the SL.

As shown in Fig. 6(c), no significant ΔEQE signal was detected under the short-circuit condition in the whole wavelength range. On the other hand, a certain level of the ΔEQE signal was obtained under reverse bias in a wide wavelength range. Note that the photon energy of the additional IR light (>1.4 μm) used for the measurements is below the gap energy between the E_- miniband (IB) and VB. Thus, the ΔEQE response is one evidence of the electron transition from the E_- miniband (IB) to the E_+ miniband (CB) induced by IR absorption. In particular, two characteristic peaks were observed at about 820 and 1000 nm, which correspond to the E_+ and E_- miniband transition energies, respectively. The ΔEQE signal at a wavelength shorter than ~820 nm is caused by repumping of electrons in the E_- miniband which are relaxed from upper states. In this sense,

the E_- miniband also behaves as an electron trap. Similar results were observed for IBSCs based on other material systems,[10,18] and thus this is a common issue to be solved for current IBSCs. The ΔEQE peak at 820 nm possibly reflects the enhanced optical absorption that originated from the VB-E_+ miniband transitions and which was observed by PR and photoluminescence excitation spectroscopies.[25–27] Therefore, although some assistance from the electric field is required, the formation of an IB structure and photocurrent generation due to sub-bandgap-photon absorption were clearly demonstrated for the solar cell with the GaAs:N δ-doped SL.

4. Conclusions

We fabricated GaAs:N δ-doped SLs by MBE and investigated their potential as an IB absorber. N content in the SLs was well controlled by adjusting the growth conditions such as the substrate temperature and N exposure time during δ-doped layer formation. SLs with average N compositions of up to 1.50% were obtained, and we succeeded in fabricating SLs with N concentrations 1 order of magnitude higher than those in the SLs fabricated by MOVPE in our previous work. The SL minibands related to E_+ and E_- bands were formed with well-separated bottom energies of up to 0.4 eV, indicating the suitability of this material system for use in IBSCs. The two-step photoabsorption process due to the electron transition from the VB to the E_+ miniband (CB) via the E_- miniband (IB) in a solar cell with a SL absorber was successfully demonstrated through EQE measurements under additional IR illumination at room temperature.

1) W. Shockley and H. J. Queisser, J. Appl. Phys. **32**, 510 (1961).
2) A. Luque and A. Martí, Phys. Rev. Lett. **78**, 5014 (1997).
3) A. Luque and A. Martí, Prog. Photovoltaics **9**, 73 (2001).
4) M. A. Green, Prog. Photovoltaics **9**, 123 (2001).
5) A. Martí, E. Antolín, C. R. Stanley, C. D. Farmer, N. López, P. Díaz, E. Cánovas, P. G. Linares, and A. Luque, Phys. Rev. Lett. **97**, 247701 (2006).
6) P. Palacios, J. J. Fernández, K. Sánchez, J. C. Conesa, and P. Wahnón, Phys. Rev. B **73**, 085206 (2006).
7) C. Tablero, Phys. Rev. B **74**, 195203 (2006).
8) R. Strandberg and T. W. Reenaas, J. Appl. Phys. **105**, 124512 (2009).
9) R. Oshima, Y. Okada, A. Takata, S. Yagi, K. Akahane, R. Tamaki, and K. Miyano, Phys. Status Solidi C **8**, 619 (2011).
10) Y. Okada, T. Morioka, K. Yoshida, R. Oshima, Y. Shoji, T. Inoue, and T. Kita, J. Appl. Phys. **109**, 024301 (2011).
11) M. Sugiyama, Y. Wang, K. Watanabe, T. Morioka, Y. Okada, and Y. Nakano, IEEE J. Photovoltaics **2**, 298 (2012).
12) P. G. Linares, A. Martí, E. Antolín, and A. Luque, J. Appl. Phys. **109**, 014313 (2011).
13) F. Wu, H. Lan, Z. Zhang, and P. Cui, J. Chem. Phys. **137**, 104702 (2012).
14) E. Cánovas, A. Martí, A. Luque, and W. Walukiewicz, Appl. Phys. Lett. **93**, 174109 (2008).
15) N. López, L. A. Reichertz, K. M. Yu, K. Campman, and W. Walukiewicz, Phys. Rev. Lett. **106**, 028701 (2011).
16) N. Ahsan, N. Miyashita, M. M. Islam, K. M. Yu, W. Walukiewicz, and Y. Okada, Appl. Phys. Lett. **100**, 172111 (2012).
17) N. Ahsan, N. Miyashita, M. M. Islam, K. M. Yu, W. Walukiewicz, and Y. Okada, IEEE J. Photovoltaics **3**, 730 (2013).
18) T. Tanaka, M. Miyabara, Y. Nagao, K. Saito, Q. Guo, M. Nishio, K. M. Yu, and W. Walukiewicz, Appl. Phys. Lett. **102**, 052111 (2013).
19) J. D. Perkins, A. Mascarenhas, Y. Zhang, J. F. Geisz, D. J. Friedman, J. M. Olson, and S. R. Kurtz, Phys. Rev. Lett. **82**, 3312 (1999).
20) W. Shan, W. Walukiewicz, J. W. Ager, III, E. E. Haller, J. F. Geisz, D. J. Friedman, J. M. Olson, and S. R. Kurtz, J. Appl. Phys. **86**, 2349 (1999).
21) W. Shan, W. Walukiewicz, K. M. Yu, J. W. Ager, III, E. E. Haller, J. F. Geisz, D. J. Friedman, J. M. Olson, S. R. Kurtz, and C. Nauka, Phys. Rev. B **62**, 4211 (2000).
22) W. Walukiewicz, W. Shan, J. Wu, K. M. Yu, and J. W. Ager, III, in *Dilute Nitride Semiconductors*, ed. M. Henini (Elsevier, Amsterdam, 2005) Chap. 10, p. 325.
23) A. Grau, T. Passow, and M. Hetterich, Appl. Phys. Lett. **89**, 202105 (2006).
24) M. Geddo, T. Ciabattoni, G. Guizzetti, M. Galli, M. Patrini, A. Polimeni, R. Trotta, M. Capizzi, G. Bais, M. Piccin, S. Rubini, F. Martelli, and A. Franciosi, Appl. Phys. Lett. **90**, 091907 (2007).
25) S. Noguchi, S. Yagi, D. Sato, Y. Hijikata, K. Onabe, S. Kuboya, and H. Yaguchi, IEEE J. Photovoltaics **3**, 1287 (2013).
26) S. Yagi, S. Noguchi, Y. Hijikata, S. Kuboya, K. Onabe, and H. Yaguchi, Jpn. J. Appl. Phys. **52**, 102302 (2013).
27) S. Yagi, S. Noguchi, Y. Hijikata, S. Kuboya, K. Onabe, Y. Okada, and H. Yaguchi, Appl. Phys. Express **7**, 102301 (2014).
28) D. E. Aspnes, Surf. Sci. **37**, 418 (1973).
29) K. Osada, T. Suzuki, S. Yagi, S. Naito, Y. Shoji, Y. Okada, Y. Hijikata, and H. Yaguchi, Tech. Dig. 6th World Conf. Photovoltaic Energy Conversion, 2014, 1.Tuo.7. 4.
30) K. Osada, T. Suzuki, S. Yagi, S. Naitoh, Y. Shoji, Y. Okada, Y. Hijikata, and H. Yaguchi, to be published in Jpn. J. Appl. Phys.
31) Web [http://www.simwindows.com].